Calibration of a Global Kinetic Mechanism Based on Synthetic Gas Bench Experiments for a Lean NOx Trap Catalyst for Automotive Applications

Calibration of a Global Kinetic Mechanism Based on Synthetic Gas Bench Experiments for a Lean NOx Trap Catalyst for Automotive Applications

F. Millo[1], M. Rafigh[1], S. Wahiduzzaman[2], R. Dudgeon[2]

[1]Dipartimento Energia, Politecnico di Torino, Italy.

E-mail: federico.millo@polito.it
Telephone: +(39) 011 090 4517
Fax: +(39) 011 090 4599

[2]Gamma Technologies Inc., Westmont, IL, USA.

E-mail: syed@gtisoft.com
Telephone: +(1) 630 325 5848

Abstract. In this paper the performance of a commercial Lean NO_x Trap (LNT), for controlling NO_x emissions in an automotive diesel engine was analyzed with the aim to investigate its catalytic properties and to build a simulation model of the aftertreament device.

In the first step, experimental tests including light-off, Oxygen Storage Capacity (OSC) and NO_x Storage and Reduction (NSR) were performed on a lab scale sample extracted from a full-scale monolith. Light-off tests have been conducted under a temperature ramp cycle from 125°C to 300°C, at a rate of 3 K/min and a space velocity of 80,000 1/hr.

OSC tests were performed with the aim to characterize the oxygen storage capacity of ceria sites and the water gas shift reaction over the precious metal, considering 10% H_2O, 5% CO_2, 0.5% O_2, and balance N_2 at the inlet during the lean phase and 10% H_2O, 2% CO and balance N_2 during the regeneration phase.

NSR experiments were then carried out by alternating a lean inlet composition to reproduce the adsorption/desorption of NO_x with a rich inlet composition fed with three different reductants H_2, CO, and C_3H_6 to replicate the NO_x reduction reactions. Both OSC and NSR were isothermal experiments performed at five different temperature levels equally spaced in 1/T starting from 150°C to 400°C and at a standard space velocity of 30,000 1/hr.

Afterwards, an LNT model was built by means of a 1-D engine simulation fluid-dynamic code, GT-Power developed by Gamma Technologies Inc., in order to assess the impact of different reaction pathways and reaction parameters. NO oxidation, NO_x adsorption/desorption, oxygen storage and NO_x reduction reactions which mainly govern the LNT operation were analyzed in detail, and reaction parameters, such as activation energies and pre-exponent multipliers, were properly calibrated using Arrhenius plot with the aim to minimize the root mean square error between simulated and experimental concentrations of NO_x and reductants (CO, H_2 and HC) in addition to N_2O and NH_3, reaching a satisfactory agreement with experimental results showing maximum 3 °C difference in light-off temperature and maximum 10% difference in prediction of NO_x conversion efficiency in the reactor scale calibrated model.

Notation

cpsi *cell per square inch.*
CFD *Computational Fluid Dynamics.*
LNT *Lean NO_x Trap.*
NSR *NO_x Storage Reduction.*
OSC *Oxygen Storage Capacity.*
PGM *Platinum Group Metals.*
SGB *Synthetic Gas Bench.*
WGS *Water Gas Shift.*

1. Introduction

One of the main issues associated to lean burn gasoline and diesel engines is attributed to the environmental concerns regarding their relatively high NO_x emissions [1], [2]. The upcoming stringent emission regulations invoke the necessity of a reliable aftertreatment system capable of reducing NO_x to levels below the legislation limit. Different aftertreatment technologies for NO_x reduction have been implemented during previous decades [3], [4] and in this context Lean NO_x Traps (LNTs), or in other words NO_x Storage Reduction (NSR) catalysts, have been introduced as a promising technology for the abatement of NO_x under lean-burn conditions [5].

The principle operation of an LNT can be described on the basis of lean/rich cyclic processes [6]. The adsorption/desorption of NO_x on the trapping component, for instance BaO, during the lean phase results in the formation of nitrates and nitrites on the catalyst surface. When the active trapping sites are saturated, a short rich phase is started by introducing a reducing agent such as H_2, CO, or HC, by means of fuel post-injection. It is noteworthy that water gas shift, steam reforming and primary oxidation of NO, producing NO_2, and the reverse reaction, producing NO from NO_2, in addition to direct reduction of NO by means of HC, CO or H_2 proceed via the presence of a precious metal, mainly Pt.

Several studies have been dedicated to the analysis of the different stages of LNT system operation. The lean phase which mainly contains the adsorption/desorption mechanisms has been investigated in several works, such as [7], [8] and [9]. On the other hand, the rich period mechanisms and the effect of using different reductants has also been extensively explored in [10], [11], [12] and [13]. As an example, Al-Harbi et al. [12] concluded that when CO is used as the reductant in wet conditions, due to the presence of water vapor, the Water Gas Shift (WGS) reaction takes place, which results in production of H_2, which can act as an additional reductant.

In the present work, the performance of a commercial Lean NO_x Trap (LNT) of an automotive diesel engine has been studied, experimentally and by simulation models, with the aim to investigate the catalytic properties of a degreened catalyst sample. Primarily, experimental activities including light-off, Oxygen Storage Capacity (OSC) and NO_x Storage and Reduction (NSR) were performed on a lab scale sample extracted from a full-scale monolith. Subsequently, the experimental results were then exploited in order to build an LNT model by means of a 1-D engine simulation fluid-dynamic code, GT-Power, in order to assess the impact of different reaction pathways which can be used for optimization purposes, control strategies and sensitivity analysis of different parameters.

2. Experimental set-up and methods

The lab scale samples were obtained from a full scale degreened monolith (the main characteristics of which are reported in Table 1) as it can be observed in Fig. 1, such that the diameter of the sample does not exceed 18.5mm.

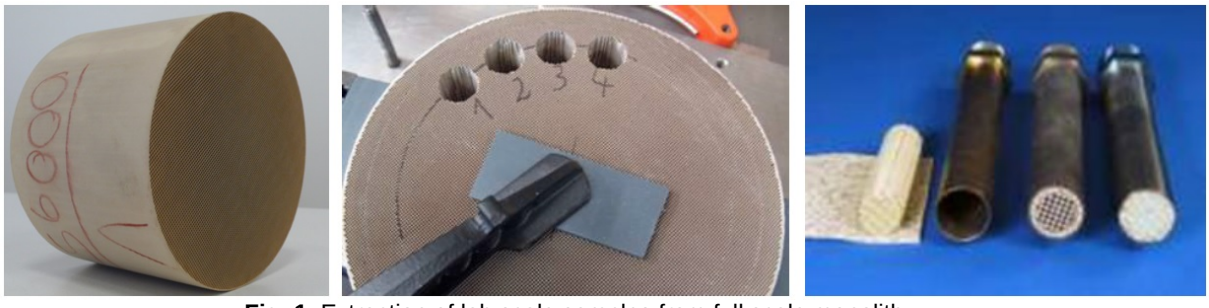

Fig. 1. Extraction of lab scale samples from full scale monolith

The experimental activity was performed at ACA – Center for Automotive Catalytic Systems of the RWTH Aachen University through a laboratory gas bench, shown in Fig. 2-a. The sample is put into an isothermal cylindrical reactor. As depicted in Fig. 2-b, two thermocouples, 0.5 mm diameter each, are mounted in the gas flow upstream, T_{US}, and downstream, T_{DS}, of the sample. Moreover, the temperatures at the sample central channel inlet, T_1, middle (3 radial positions, T_2, T_4, T_5), and outlet, T_3, have also been measured.

Gas concentration measurements were performed with a multicomponent FTIR with 1 Hz sampling frequency.

Since H_2 measurements were not available downstream of the catalyst, the predicted catalyst outlet H_2 concentration from simulation model could be validated only indirectly by checking the other species concentrations.

Table 1. Main characteristics of the LNT under investigation

Characteristic	Unit	Value
Substrate material	-	Cordierite
Cell density	cpsi	400
Wall thickness	mil	4
Dimensions (short radius x long radius x length)	mm	68.58 x 68.58 x 96.6
PGM loading	g/ft^3	120
PGM ratio (Pt:Pd:Rh)	-	103:12:5

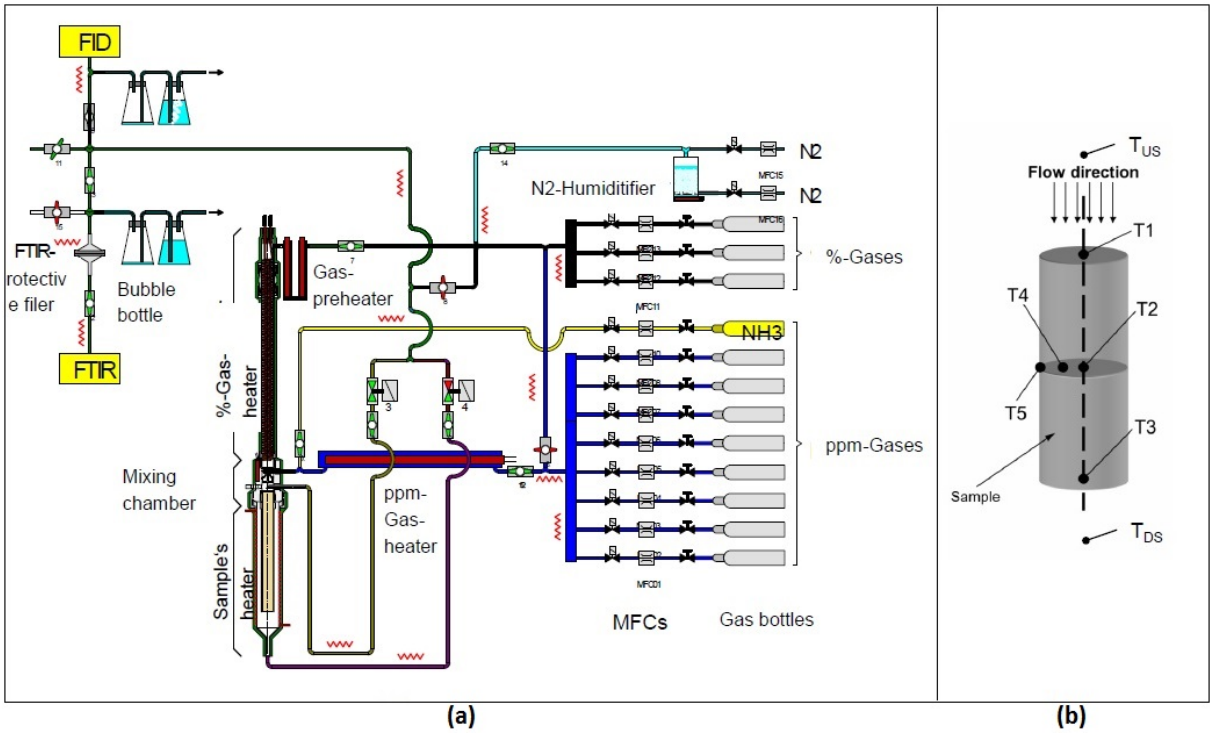

Fig. 2. Experimental setup: schematic view of laboratory gas bench (a) and thermocouple locations on the lab scale sample (b)

2.1 Light-off test

The light-off behavior of the catalyst during warm-up can be examined by means of light-off experiments through a temperature ramp cycle which gives the possibility to predict the CO and HC oxidation rates on the noble metal component as a function of the catalyst temperature [14]. The temperature ramp cycle starts from 125°C to 300°C at a rate of 3 K/min. The experiment is performed at a space velocity of 80,000 1/hr with the inlet feed composition shown in Table 2. HCs are specified on a C3 basis and consist of a 2:1 molar ratio of propane (C_3H_8) to propylene (C_3H_6).

2.2 Oxygen Storage Capacity (OSC) test

Thanks to the presence of ceria on the washcoat layer, the LNT demonstrates oxygen storage capacity. Ceria loading promotes water gas shift reaction activity and therefore favors H_2 formation under rich conditions [12], [15], [16] which facilitates catalyst regeneration.

The OSC experiment is performed at a space velocity of 30,000 1/hr with a sufficient pre-reduction with H_2 prior to each test run, 900 seconds. Five inlet temperatures, starting from 150 °C to 450 °C are tested.

OSC consists of a lean phase and a short rich phase by introduction of CO as the reducing agent. Overlap between feeding oxygen and CO simultaneously is avoided by waiting to feed CO until oxygen is completely shut-off. The inlet gas composition is presented in Table 3.

Table 2. Inlet gas composition for light-off experiments in (concentrations on volume basis)

Species	Composition
HC [ppm]	400
CO [ppm]	300
H_2 [ppm]	60
O_2 [%]	10
CO_2 [%]	5
H_2O [%]	5
N_2	Balance

Table 3. Inlet gas composition for OSC experiments (concentrations on volume basis)

Species	Lean phase (60 s)	Rich phase (30 s)
CO [ppm]	0	20000
O_2 [%]	0.5	0
CO_2 [%]	5	0
H_2O [%]	10	10
N_2	Balance	Balance

2.3 NOx Storage Reduction (NSR) test

Finally, main characteristic of the LNT which includes the NO_x adsorption/desorption during lean phase and NO_x reduction during rich phase is explored by means NSR experiments [10] , [17].

The NSR test is carried out at a space velocity of 30,000 1/hr and a sufficient pre-reduction with H_2 prior to each reactor run, 900 seconds. Five inlet temperatures, starting from 150 °C to 400 °C, are tested which are equally spaced in 1/T, where T is in Kelvin. The experiment is ideally repeated at each temperature using H_2, CO, and HC (represented by propylene) as reductant for each step. The inlet gas composition for lean/rich cycle is reported in Table 4.

Table 4. Inlet gas composition for NSR experiments (concentrations on volume basis)

Species	Lean	Rich, H_2	Rich, CO	Rich, HC
Reductant [ppm]	0	1000	1000	110
O_2 [%]	10	0	0	0
CO_2 [%]	5	5	5	5
H_2O [%]	5	5	5	5
NO [ppm]	300	0	0	0
N_2	Balance	Balance	Balance	Balance

Since engine-out NO_x emission mainly consists of NO, in the NSR test protocol inlet NO_x only includes NO, although NO_2 adsorption/desorption kinetics can be indirectly characterized due to production of NO_2 from oxidation of NO.

3. Simulation model

The LNT model was built at first for the reactor scale sample, i.e. for a cylinder of 18 mm diameter and a length of 96.6 mm, corresponding to the full monolith length.

The reaction mechanism is a global-type surface reaction mechanism using Turnover Number reaction rate format. It incorporates the NO oxidation, NO_x adsorption/desorption on barium sites, oxygen storage on ceria and NO_x reduction reactions in addition to WGS and steam reforming reaction taking place over PGM.

The reaction rates can be expressed by general form of Arrhenius term as expressed in Equation 1:

$$R_i = \frac{A_i \exp(-\frac{E_{ai}}{RT}) C_i \theta}{G_i} \quad (1)$$

in which:

- R represents the rate of reaction i
- A and E_a stand for pre-exponent multiplier and activation energy, respectively
- G accounts for inhibition terms, if required, and C represents the reactant concentrations in mol/m^3
- θ stands for the surface site coverage varying between 0 to 1

Calibration of the model is performed with the aim of minimizing an objective function:

$$Objective(Error)Function = \int_0^{t_{end}} | C_{measured} - C_{simulated} |_{species} dt \quad (2)$$

The calibration parameters, or independent variables, include site densities, pre-exponent multiplier and activation energy for each reaction. Since the OSC and NSR tests are performed at constant temperature steps, Arrhenius plot can be used for characterizing the pre-exponent multiplier and activation energy for each reaction. Therefore, calibration is performed starting from the lowest temperature and moving to the next highest temperature; at each temperature an optimal rate is found without temperature dependency and the temperature dependency is determined by using the Arrhenius plot to yield an activation energy as it can be observed in Fig. 3.

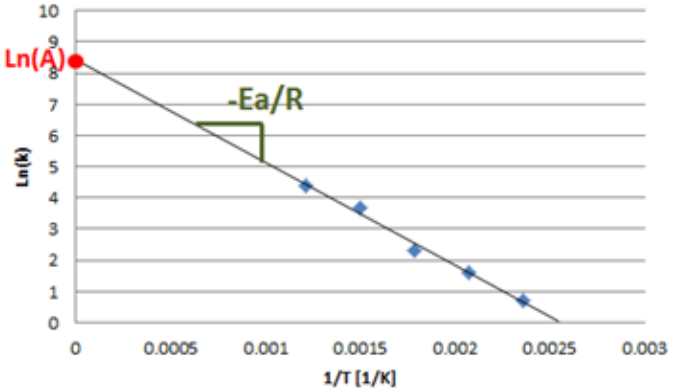

Fig. 3 Arrhenius plot used for calibration

More details regarding the calibration approach can be found in [18].

3.1 OSC model

The reactions in this step include the storage of oxygen on ceria site during lean phase and the reduction of stored oxygen by means of CO during rich phase.

In addition, due to the presence of H_2O in the inlet feed, during rich phase H_2 is produced as a result of WGS reaction over the precious metal Pt. The reaction mechanism can be described as reported in Table 5.

Table 5. Reaction mechanisms for OSC experiments

#	Site	Reaction
1	ceria	$Ce_2O_3 + 0.5O_2 \rightarrow 2CeO_2$
2	ceria	$CeO_2 + CO \rightarrow Ce_2O_3 + CO_2$
3	ceria	$CeO_2 + H_2 \rightarrow Ce_2O_3 + H_2O$
4	ceria	$2CeO_2 + 1/9C_3H_6 \rightarrow Ce_2O_3 + 1/3CO_2 + 1/3H_2O$
5	PGM	$CO + H_2O \leftrightarrow CO_2 + H_2$

Thanks to the fact that CO_2 is not injected during rich phase, all the CO_2 measured at the outlet can be related to WGS reaction, which is utilized for the calibration of WGS reaction.

Considering the H_2 and HC reactions in OSC test, since the test protocol does not include HC and H_2 at the inlet batch, a preliminary value from literature was used which was further tuned during NSR test focusing on the reductant breakthrough.

The optimized pre-exponent multipliers and activation energies for OSC reaction mechanisms are expressed in Table 6.

It is worth noting that the reactions on PGM are inhibited by Voltz-type inhibition function with following equation:

$$G_{voltz} = G_1 \times G_2 \times G_3 \tag{3}$$

In which:

$$G_1 = \frac{1}{(1 + 9.467\exp(63.451/\mathrm{T})\ \mathrm{C_{CO}} + 274.82\exp(-215.34/\mathrm{T})\ \mathrm{C_{C_3H_6}})^2} \tag{4}$$

$$G_2 = \frac{1}{(1 + 0.00061\exp\ (9715.6/\mathrm{T})\ \ \mathrm{C_{CO}}^2\mathrm{C_{C_3H_6}}^2)} \tag{5}$$

$$G_2 = \frac{1}{(1 + 5.554\mathrm{E6}\exp(-6206.9/\mathrm{T})\ \mathrm{C_{NO}})} \tag{6}$$

Table 6. Optimized pre-exponent multiplier and activation energy for OSC test

#	Pre-exponent Multiplier	Activation Energy [J/mol]
1	0.1	0
2	3.2	$1800(1-0.9\theta_{CeO_2})$
3	12.6	$2900(1-0.7\theta_{CeO_2})$
4	0.06	$1800(1-0.9\theta_{CeO_2})$
5	3.24E6	61000

3.2 Light-off model

As far as light-off experiments modelling are considered, the reaction mechanism [19] includes the previously calibrated reactions using OSC tests, (see Table 5), in addition to oxidation of CO, HC and H_2 and steam reforming reactions which are presented in Table 7, including the pre-exponent multiplier and activation energy obtained for each reaction.

Table 7. Reaction mechanisms for light-off experiments

#	Site	Reaction	Pre-exponent Multiplier	Activation Energy [J/mol]
1	PGM	$CO + 0.5O_2 \rightarrow CO_2$	1E13	88190
2	PGM	$H_2 + 0.5O_2 \rightarrow H_2O$	1.8E15	111450
3	PGM	$C_3H_6 + 4.5O_2 \rightarrow 3CO_2 + 3H_2O$	1E15	104600
4	PGM	$C_3H_8 + 5O_2 \rightarrow 3CO_2 + 4H_2O$	1.5E6	71100
5	PGM	$C_3H_6 + 3H_2O \rightarrow 3CO + 6H_2$	6E8	89200
6	PGM	$C_3H_8 + 3H_2O \rightarrow 3CO + 7H_2$	1.2E13	174200

3.3 NSR model

During NO_x storage phase the reaction mechanism includes NO oxidation on the PGM and NO_x adsorption/desorption on the barium sites, in the form of barium nitrates and barium nitrites, using the reaction pathway exploited by [20].

$$NO + 0.5O_2 \leftrightarrow NO_2 \quad (7)$$

$$BaO + 2NO + 1.5O_2 \leftrightarrow Ba(NO_3)_2 \quad (8)$$

$$BaO + 2NO_2 + 0.5O_2 \leftrightarrow Ba(NO_3)_2 \quad (9)$$

$$BaO + 2NO + 0.5O_2 \leftrightarrow Ba(NO_2)_2 \quad (10)$$

$$BaO + 3NO_2 \rightarrow Ba(NO_3)_2 + NO \quad (11)$$

$$Ba(NO_2)_2 + 0.5O_2 \rightarrow Ba(NO_3)_2 \quad (12)$$

In order to take into account the non-monotonic storage capacity of barium sites with respect to temperature, multiple-adsorption site model was considered [9], [21], including three kinds of barium sites which differ in the active site density. It was observed that, for temperatures lower than 210 °C, two types of barium sites are sufficient, while at higher temperatures the third kind of barium site is activated, which is inhibited by NO at lower temperatures with a function G defined as:

$$\mathrm{G} = \frac{1}{1 + 0.000226175\exp(10190/\mathrm{T})\mathrm{C}_{\mathrm{NO}}} \quad (13)$$

As far as reduction reactions are considered, due to the production of H_2 from WGS and steam reforming reactions when CO and C_3H_6 are used as the reductant, respectively, the calibration is started from the cases where H_2 is used as the primary reductant. In this case the reaction mechanism is set according to [22], [23], [24].

$$Ba(NO_3)_2 + 8H_2 \rightarrow BaO + 2NH_3 + 5H_2O \quad (14)$$

$$Ba(NO_3)_2 + \frac{10}{3}NH_3 \rightarrow BaO + \frac{8}{3}N_2 + 5H_2O \quad (15)$$

$$Ba(NO_3)_2 + 2NH_3 \rightarrow BaO + 2N_2O + 3H_2O \quad (16)$$

$$Ba(NO_2)_2 + \frac{2}{5}NH_3 \rightarrow BaO + \frac{12}{5}NO + \frac{3}{5}H_2O \quad (17)$$

Other reaction mechanisms include the reduction of stored NO_x by CO and propylene producing NO and N_2 on barium sites and over the precious metal.

The calibration is performed step by step as follows:

1. NO_x storage
2. NO_x reduction, H_2 reductant
3. NO_x reduction, CO reductant
4. NO_x reduction, C_3H_6 reductant

In each step, the calibration is performed moving from lower to higher temperature cases using Arrhenius rate functions.

4. Results and discussions

The result of OSC calibration model for each inlet temperature is shown in Fig. 4, considering that the start of the rich phase is characterized by the injection of CO as the reductant.

The production of CO_2 as a result of water gas shift reaction is predicted with good accuracy, which increases by increasing temperature, such that at higher temperatures all CO is converted to H_2 and CO_2. Moreover, CO breakthrough which takes into account the stored O_2 clean-off from ceria sites matches the experimental data with satisfactory accuracy.

Considering light-off test, results are shown in Fig. 5. It can be observed that both the concentrations and the conversion efficiencies are in good agreement with experimental data. As expected, the slow oxidizing HC, in this case propane, does not reach light-off until 370 °C.

In more detail, light-off temperatures based on 80% conversion efficiency are reported in Fig. 6. The error between simulated and experimental light-off temperatures does not exceed 4 °C. It is noteworthy that since CO light-off temperature considering 50% conversion could be lower than the minimum temperature used in this test, 80% efficiency level was selected for light-off definition.

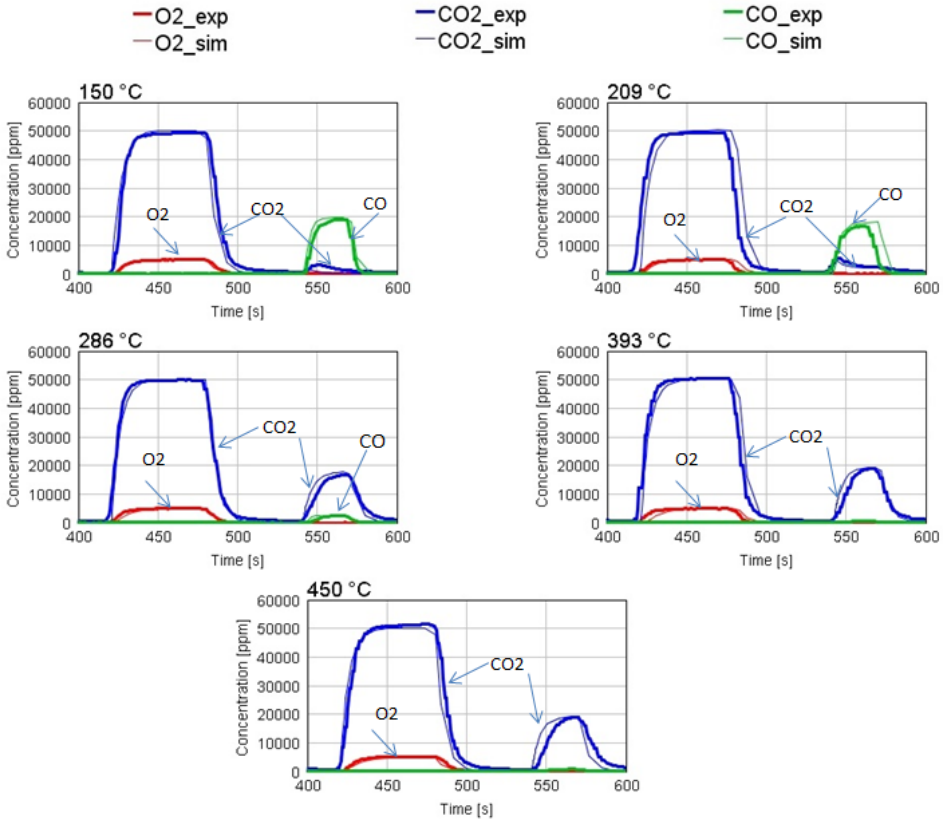

Fig. 4. OSC calibrated simulation model results in comparison with experimental data

This behavior can, at least in part, be attributed to the fact that the light-off inlet batch does not include NO, which typically shows an inhibition effect over the PGM: hence with the presence of NO, all light-off temperatures would be shifted to higher values. Moreover, the presence of considerable amount of H_2 in the inlet batch of light-off (CO/H_2 = 300/60 = 5), Table 2, affects strongly CO and HC oxidation and thus their light-off temperature [25].This effect can be furtherly investigated by performing SGB tests with different H_2 concentrations.

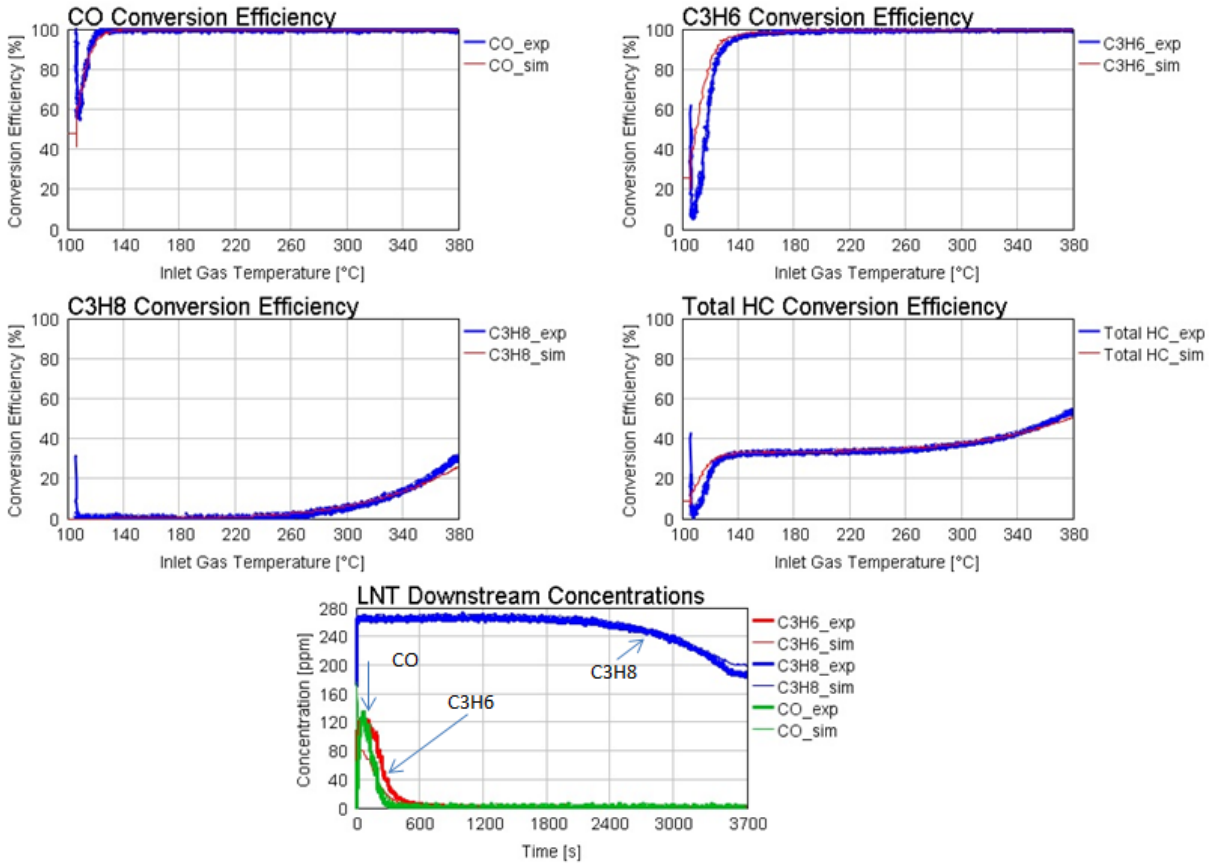

Fig. 5. Light-off calibrated simulation model results in comparison with experimental data

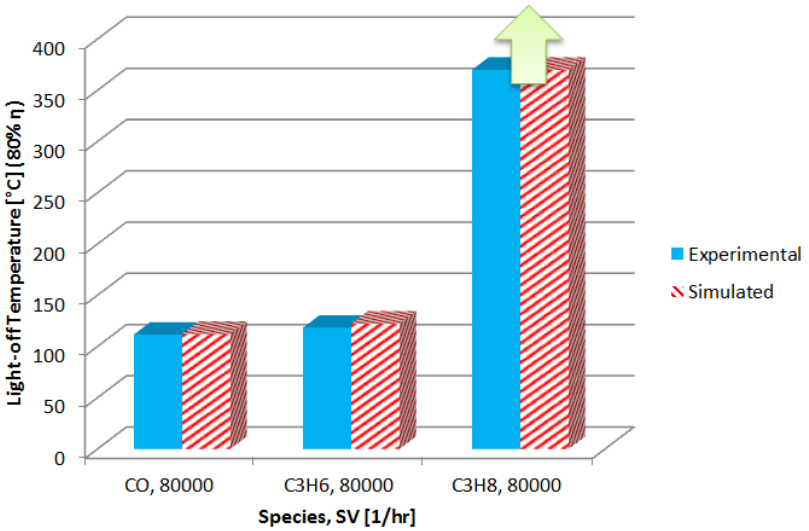

Fig. 6. Comparison of simulation and experimental light-off temperature based on 80% efficiency

As far as NSR tests are concerned, the results considering H_2, CO and C_3H_6 reductants are shown in Fig. 7, Fig. 8 and Fig. 9, respectively.

It is worth noting that the NO and NO_2 concentrations during regeneration phase is identical to experimental data considering all the three reductants injected during rich pulse. Besides, it has been

found out that C_3H_6 is less efficient in terms of NO_x slip abatement during reduction phase [26], specifically at low temperatures as shown in Fig. 9.

Furthermore, it can be appreciated that even when CO and C_3H_6 are used as the primary reductants, the main share of regeneration is carried out by H_2 as a result of WGS and steam reforming reactions, specifically at higher temperatures where H_2 production is favored.

It should be noted also that at 193 °C when propylene is used as the primary reductant, the NO concentration resulting from simulation is over estimated. However, this mismatching could be, at least in part, attributed to experimental errors. Due to the fact that the test rig is not fully automated, the storage part in this case is not identical with other experiments at 193 °C, hence the simulation model apparently over estimates the NO outlet concentration.

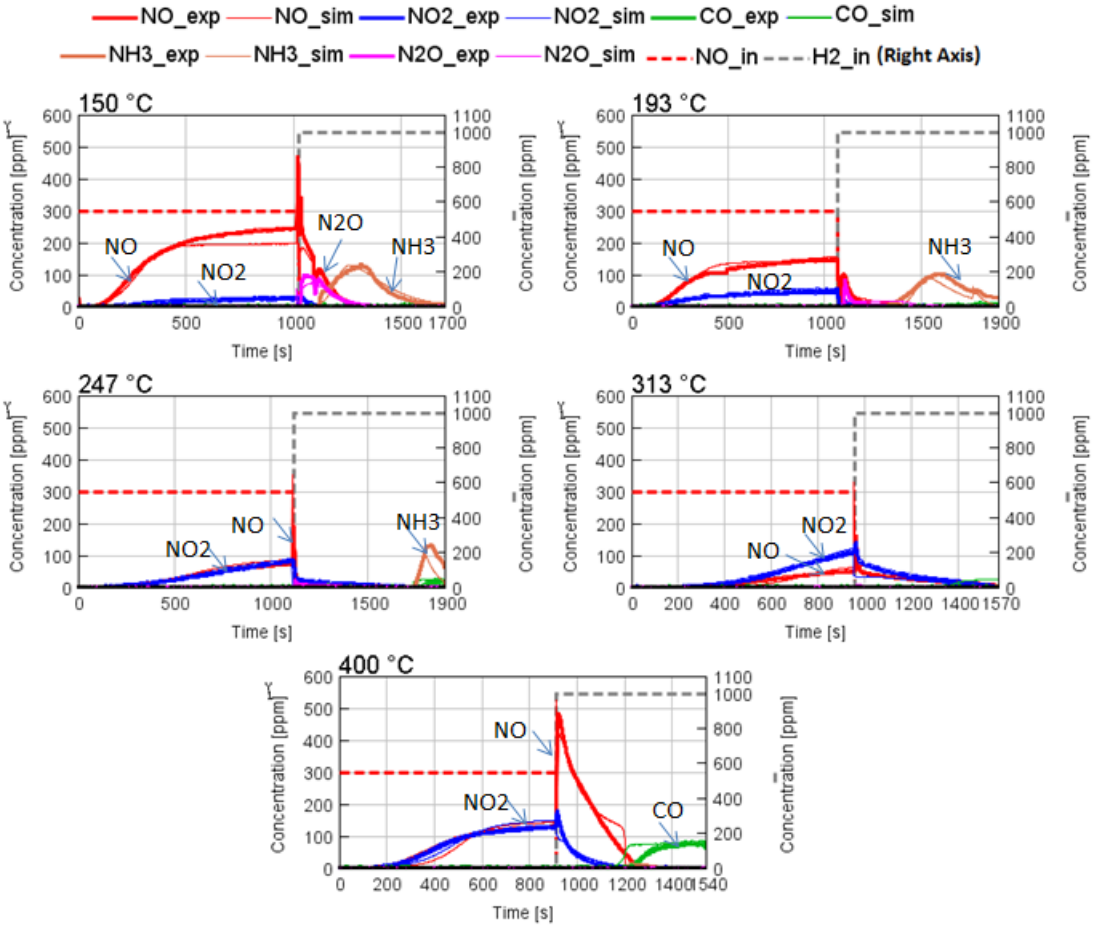

Fig. 7. NSR calibrated simulation model results in comparison with experimental data (H_2 used as reductant)

In addition, average site coverages for the three barium sites are presented in Fig. 10 during NSR test in which CO is used as the primary reductant. It can be observed that site coverages decrease during storage phase due to adsorption of NO_x species on barium. Afterwards, during rich pulse in which reductant is injected, adsorption capacity of the system is recovered.

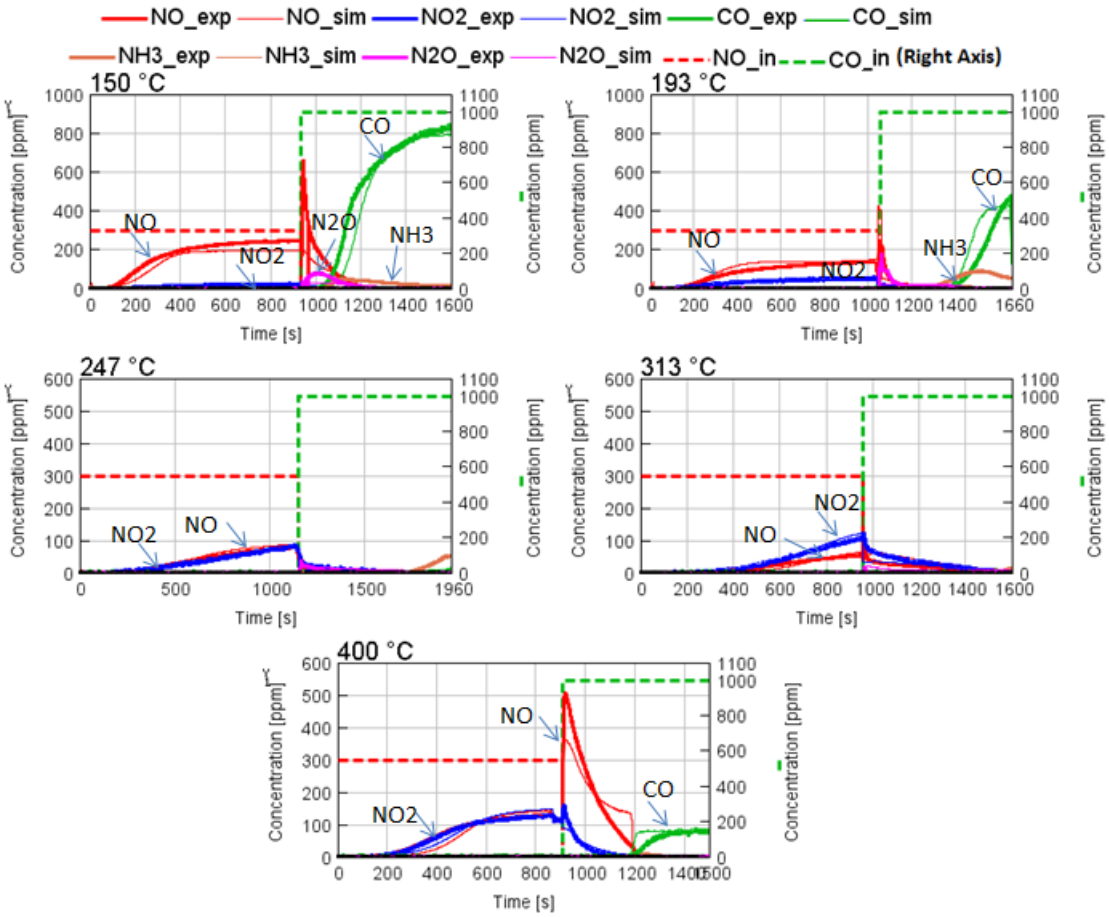

Fig. 8. NSR calibrated simulation model results in comparison with measured data (CO used as reductant)

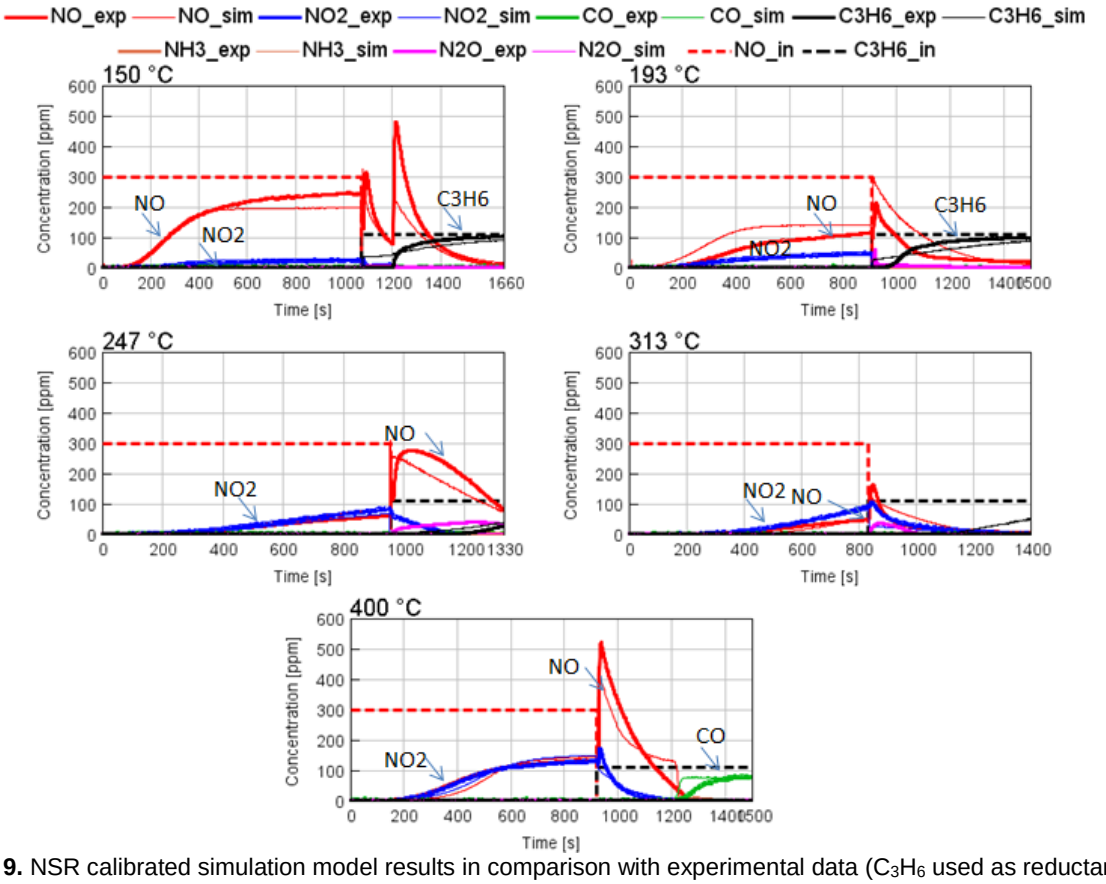

Fig. 9. NSR calibrated simulation model results in comparison with experimental data (C_3H_6 used as reductant)

The comparison between experimental and predicted NO_x conversion efficiency is depicted in Fig. 11. The simulation results show acceptable matching with experimental data with maximum difference not exceeding 10%, if the excluding the case in which propylene was used as the primary reductant at 193 °C, due to the experimental error already discussed. It can be observed that at low temperatures H_2 is the most effective reductant, reaching 32% and 38% of conversion efficiency from measured data and simulation model, respectively, exhibiting higher NO_x conversion with respect to CO and propylene.

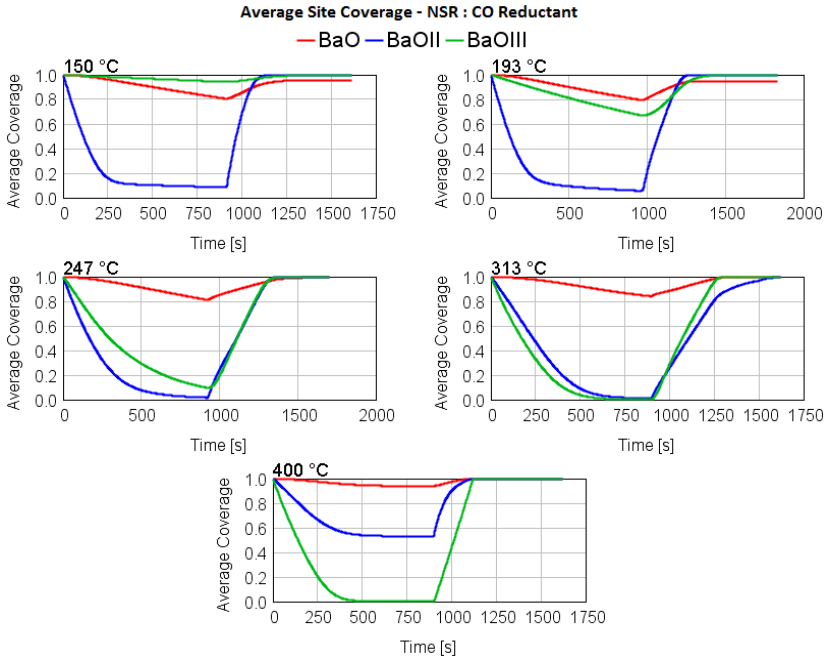

Fig. 10. Average barium site coverages during NSR test when CO is used as the primary reductant

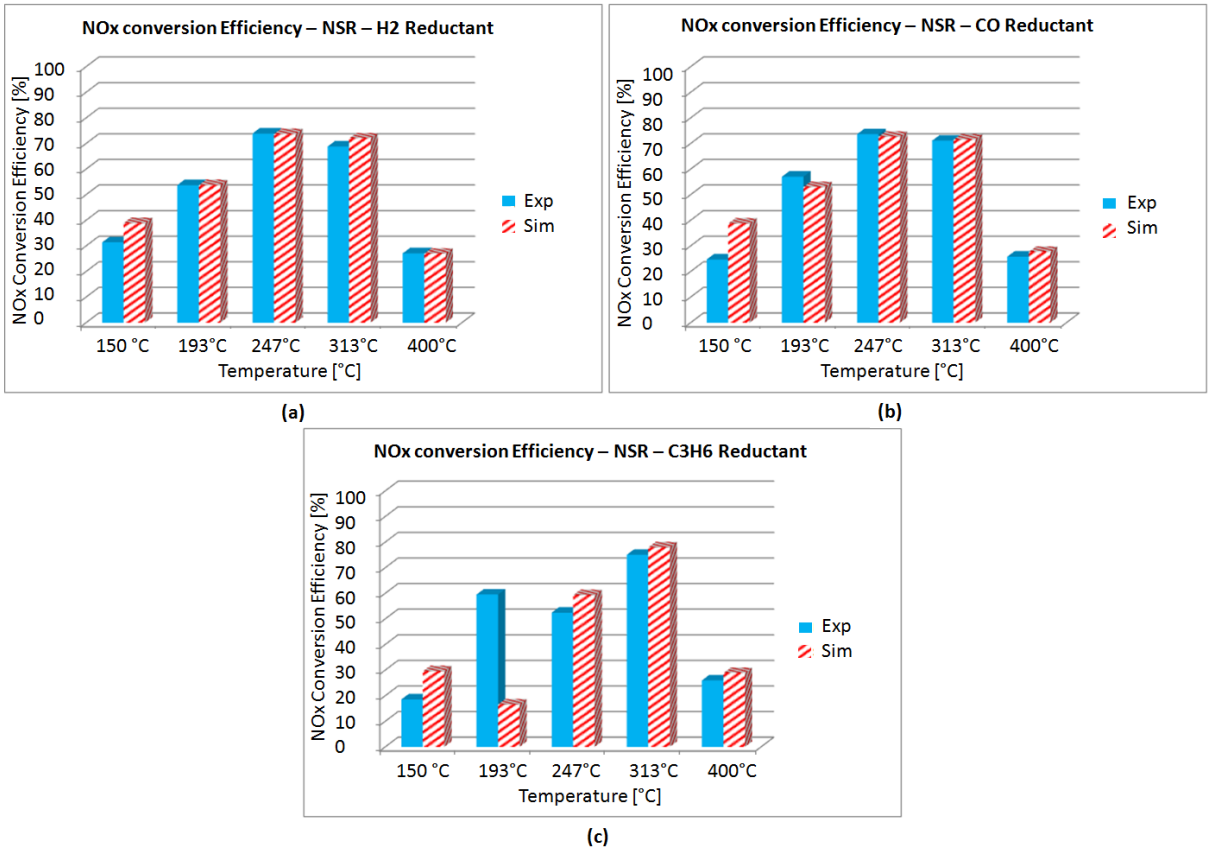

Fig. 11. Comparison between predicted and experimental NO_x conversion efficiency using different reductants H_2 (a), CO (b) and C_3H_6 (c)

Conclusions

In the present work, the catalytic properties of a commercial Lean NO_x Trap of the $Pt/BaO/Al_2O_3$ type for controlling NO_x emissions in an automotive diesel engine have been investigated experimentally and numerically.
The light-off, Oxygen Storage Capacity (OSC), NO_x Storage and Reduction (NSR) experiments were performed on a lab scale sample extracted from a full-scale monolith at standard space velocity of 30,000 1/hr and 5 constant inlet temperatures starting from 150 °C to 400 °C, spaced equally in 1/T in order to simplify the determination of temperature dependent rate constants. The NO_x reduction tests were carried out considering three types of reductants: H_2, CO and C_3H_6.

Afterwards, a 1-D CFD simulation model of the LNT catalyst was built by using a commercially available software, GT-Power developed by Gamma Technologies Inc. The model was calibrated and the optimized calibration parameters including the ceria and barium site densities, pre-exponent multipliers and the activation temperature of each reaction were found aiming to minimize the Mean Square error between simulated and experimental concentrations of the reaction products downstream of the catalyst.

After a first calibration of the model for the OSC and light-off experiments, the model was calibrated for the NO_x storage experiment by considering three kinds of barium sites with different site densities in order to take into account the non-uniformity of barium sites distribution. It is worth noting that the third barium site is activated at temperatures higher than 210 °C and is inhibited by NO at lower temperatures. NO_x adsorption/desorption over the barium sites in addition to NO oxidation on Pt which mainly govern the lean phase were calibrated. At the end, the rich phase was modelled starting from the tests where H_2 was injected as the primary reductant, since H_2 is produced as a result of WGS and steam reforming reactions when CO or C_3H_6 are injected, respectively.

In addition, it was realized that due to presence of water vapor in the inlet batch, WGS and steam reforming result in high production of H_2 even when CO and C_3H_6 are used as the primary reductants; subsequently, the main share of regeneration is carried out by H_2, specifically at higher temperatures. Moreover, propylene presented a lower effectiveness in terms of NO_x slip abatement during reduction phase.

At the end, it is worth pointing out that the simulation results coming from the LNT calibrated model for the lab scale component indicated acceptable accuracy with experimental data, with a maximum error of 4 °C in terms of light-off temperature prediction and maximum relative error of 10% in NO_x conversion efficiency.

Future activity will therefore be dedicated to the refinement of the simulation model for the full-scale component, aiming to validate the predictive capability of the LNT model and assess the performance of the component over driving cycles. Moreover, the analysis of the effect the sulphur content on the LNT performance, both experimentally and analytically, is a part of future investigations.

References

[1] Forzatti, P., Lietti, L., Gabrielli, N., "A kinetic study of the reduction of NOx stored on Pt-Ba/Al2O3 catalyst," *Applied Catalysis B: Environmental*, vol. 99, no. 1-2, pp. 145-155, August 2010, 10.1016/j.apcatb.2010.06.011.

[2] Epling, W.S., Campbell, L.E., Yezerets, A., Currier, N.W., et al., "Overview of the fundamental reactions and degradation mechanisms of NOx storage/reduction catalysts," *Catalysis Reviews - Science and Engineering*, vol. 46, no. 2, pp. 163-245, 2004, 10.1081/CR-200031932.

[3] Liu, Z., Woo, S.I., "Recent Advances in Catalytic DeNOX Science and Technology," *Catalysis Reviews: Science and Engineering*, vol. 48, no. 1, pp. 43-89, 2006, 10.1080/01614940500439891.

[4] Forzatti, P., Lietti, L., Nova, I., Tronconi, E., "Diesel NOx aftertreatment catalytic technologies: Analogies in LNT and SCR catalytic chemistry," *Catalysis Today*, vol. 151, no. 3-4, pp. 202-211, June 2010, 10.1016/j.cattod.2010.02.025.

[5] Nova, I., Castoldi, L., Lietti, L., Tronconi, E., et al., "The Pt-Ba Interaction in Lean NOx Trap Systems," in *SAE Technical Paper*, 2005.

[6] Tonkyn, R.G., Disselkamp, R.S., Peden, C.H.F., "Nitrogen release from a NOx storage and reduction catalyst," *Catalysis Today*, vol. 114, no. 1, pp. 94-101, 2006, 10.1016/j.cattod.2006.02.005.

[7] Daw, C.S., Chakravart, K., Lenox, K.E., "A simple model for lean NOx adsorber catalysts," in *CLEERS*, 2002.

[8] Xu, J., Harold, M.P., Balakotaiah, V., "Modeling the effects of Pt loading on NOx storage on Pt/BaO/Al2O3 catalysts," *Applied Catalysis B: Environmental*, vol. 104, no. 3-4, pp. 305-315, May 2011, 10.1016/j.apcatb.2011.03.014.

[9] Epling, W.S., Parks, J.E., Campbell, G.C., Yezerets, A., et al., "Further evidence of multiple NOx sorption sites on NOx storage/reduction catalysts," *Catalysis Today*, vol. 96, no. 1-2, pp. 21-30, October 2004, 10.1016/j.cattod.2004.05.004.

[10] Nova, I., Lietti, L., Forzatti, P., Prinetto, F., et al., "Experimental investigation of the reduction of NOx species by CO and H2 over Pt–Ba/Al2O3 lean NOx trap systems," *Catalysis Today*, vol. 151, no. 3-4, pp. 330-337, June 2010, 10.1016/j.cattod.2010.02.075.

[11] Morandi, S., Ghiotti, G., Castoldi, L., Lietti, L., et al., "Reduction by CO of NOx species stored onto Pt–K/Al2O3 and Pt–Ba/Al2O3 lean NOx traps," *Catalysis Today*, vol. 176, no. 1, pp. 399-403, November 2011, 10.1016/j.cattod.2010.11.024.

[12] AL-Harbi, M., Epling, W.S., "The effects of regeneration-phase CO and/or H2 amount on the performance of a NOX storage/reduction catalyst," *Applied Catalysis B: Environmental*, vol. 89, no. 3-4, pp. 315-325, July 2009, DOI: 10.1016/j.apcatb.2008.12.010, http://dx.doi.org/10.1016/j.apcatb.2008.12.010.

[13] Masdrag, L., Courtois, X., Can, F., Royer, S., et al., "Understanding the role of C3H6, CO and H2 on efficiency and selectivity of NOx storage reduction (NSR) process," *Catalysis Today*, vol. 189, no. 1, pp. 70-76, July 2012, 10.1016/j.cattod.2012.03.053.

[14] Duprat, F., "Light-off curve of catalytic reaction and kinetics," *Chemical Engineering Science*, vol. 57, no. 6, pp. 901-911, March 2002, 10.1016/S0009-2509(01)00409-2.

[15] Phatak, A.A., Koryabkina, N., Rai, S., Ratts, J.L., Ruettinger, W., Farrauto, R.J., Blau, G.E., Delgass, W.N., Ribeiro, F.H., "Kinetics of the water–gas shift reaction on Pt catalysts supported on alumina and ceria," *Catalysis Today*, vol. 123, no. 1–4, pp. 224-234, 2007, http://dx.doi.org/10.1016/j.cattod.2007.02.031. .

[16] Jacobs, G., Williams, L., Graham, U., Thomas, G.A., Sparks, D.E., Davis, B.H., "Low temperature water–gas shift: in situ DRIFTS-reaction study of ceria surface area on the evolution of formates on Pt/CeO2 fuel processing catalysts for fuel cell applications," *Applied Catalysis A: General*, vol. 252, no. 1, pp. 107-118, 2003, http://dx.doi.org/10.1016/S0926-860X(03)00410-1.

[17] Koop, J. and Deutschmann, O., "Modeling and Simulation of NOx Abatement with Storage/Reduction Catalysts for Lean Burn and Diesel Engines," in *SAE Technical Paper*, 2007.

[18] GT-SUITE Aftertreatment Manual, Gamma Technologies, 2014.

[19] Ramanathan, K., Sharma, C.S., "Kinetic Parameters Estimation for Three Way Catalyst Modeling," *Industrial & Engineering Chemistry Research*, vol. 50, no. 17, pp. 9960-9979, 2011, DOI: 10.1021/ie200726j, http://dx.doi.org/10.1021/ie200726j.

[20] Forzatti, P., Lietti, L., Nova, I., Morandi, S., et al., "Reaction pathway of the reduction by CO under dry conditions of NOx species stored onto PtBa/Al2O3 Lean NOx Trap catalysts," *Journal of Catalysis*, vol. 274, no. 2, pp. 163-175, 2010, 10.1016/j.jcat.2010.06.014.

[21] Mahzoul, H., Brilhac, J.F., Gilot, P., "Experimental and mechanistic study of NOx adsorption over NOx trap catalysts," *Applied Catalysis B: Environmental,* vol. 20, no. 1, pp. 47-55, January 1999, DOI: 10.1016/S0926-3373(98)00093-9, http://dx.doi.org/10.1016/S0926-3373(98)00093-9.

[22] Kočí, P., Schejbal, M., Trdlička, J., Gregor, T., et al., "Transient behaviour of catalytic monolith with NOx storage capacity," *Catalysis Today,* vol. 119, no. 1-4, pp. 64-72, January 2007, 10.1016/j.cattod.2006.08.014.

[23] Shwan, S., Partridge, W., Choi, J.S., Olsson, L., "Kinetic modeling of NOx storage and reduction using spatially resolved MS measurements," *Applied Catalysis B: Environmental,* vol. 147, pp. 1028-1041, 2014, DOI: 10.1016/j.apcatb.2013.10.023, http://dx.doi.org/10.1016/j.apcatb.2013.10.023.

[24] Lindholm, A., Currier, N.W., Li, J., Yezerets, A., Olsson, L., "Detailed kinetic modeling of storage and reduction with hydrogen as the reducing agent and in the presence of CO2 and H2O over a Pt/Ba/Al catalyst,, Volume," *Journal of Catalysis,* vol. 258, no. 1, pp. 273-288. DOI: 10.1016/j.jcat.2008.06.022, http://dx.doi.org/10.1016/j.jcat.2008.06.022.

[25] Lindholm, A., Currier, N.W., Fridell, E., Yezerets, A., Olsson, L., "NOx storage and reduction over Pt based catalysts with hydrogen as the reducing agent: Influence of H2O and CO2," *Applied Catalysis B: Environmental,* vol. 75, no. 1-2, pp. 78-8, 2007, DOI: 10.1016/j.apcatb.2007.03.008, http://dx.doi.org/10.1016/j.apcatb.2007.03.008.

[26] Kočí, P., Novák, V., Štěpánek, F., Marek, M., Kubíček, M., "Multi-scale modelling of reaction and transport in porous catalysts," *Chemical Engineering Science,* vol. 65, no. 1, pp. 412-419, 2010, DOI: 10.1016/j.ces.2009.06.068, http://dx.doi.org/10.1016/j.ces.2009.06.068.

[27] Kryl, D., Kočí, P., Kubíček, M., Marek, M., Maunula, T., Härkönen, M, "Catalytic Converters for Automobile Diesel Engines with Adsorption of Hydrocarbons on Zeolites," *Industrial & Engineering Chemistry Research,* vol. 44, no. 25, pp. 9524-9534, 2005, DOI: 10.1021/ie050249v, http://dx.doi.org/10.1021/ie050249v.

[28] Wehinger, G.D., Eppinger, T., Kraume, M., "Fluidic effects on kinetic parameter estimation in lab-scale catalysis testing – A critical evaluation based on computational fluid dynamics," *Chemical Engineering Science,* vol. 111, pp. 220-230, 2014, DOI: 10.1016/j.ces.2014.02.025, http://dx.doi.org/10.1016/j.ces.2014.02.025.

[29] Katare, S. and Laing, P., "Hydrogen in Diesel Exhaust: Effect on Diesel Oxidation Catalyst Flow Reactor Experiments and Model Predictions," *SAE International Journal of Fuels and Lubricants. J. Fuels Lubr,* pp. 605-611, 2009, DOI:10.4271/2009-01-1268.